# Spin Nernst and anomalous Nernst effects and their signature outputs in ferromagnet/nonmagnet heterostructures

Chi Sun,* S M Rafi-Ul-Islam, Hyunsoo Yang, and Mansoor B. A. Jalil†
*Department of Electrical and Computer Engineering, National University of Singapore, 117576 Singapore*

(Received 26 May 2020; revised 23 November 2020; accepted 28 November 2020; published 15 December 2020)

The spin Nernst effect (SNE) and anomalous Nernst effect (ANE) convert a heat current generated by a temperature gradient to a spin current in nonmagnetic metals and ferromagnets, respectively. We present a diffusive spin transport theory of the combination of these thermoelectric effects in ferromagnet (F)/nonmagnet (N) heterostructures and their respective output signals. In a F/N bilayer, in the presence of an in-plane temperature gradient, electrical voltages are induced by the SNE in N and the ANE in the F layers, via the inverse spin Hall effect in the N. The analytical expression of the thermally driven spin Hall magnetoresistance (TSMR) output is derived, which captures both the local SNE contribution in the N and the nonlocal mixing contribution due to the ANE in the adjacent F. Interestingly, the SNE and ANE give additive contributions to the transverse TSMR voltages but subtract from each other for the longitudinal component. This anisotropic response suggests a possible means to extract the individual SNE and ANE contributions, as well as spin-dependent polarization parameters. In a F1/N/F2 trilayer, both SNE and ANE contribute to spin torques on the free F2 layer. We analyze the ferromagnetic resonance (FMR) of the free layer and show that both thermoelectric effects contribute additively to the FMR magnitude and linewidth for the considered magnetization configuration. Finally, we show that TSMR can provide a more sensitive experimental detection of SNE and ANE down to a threshold thermal gradient of the order of $10^{-6}$ K/nm.

DOI: 10.1103/PhysRevB.102.214419

## I. INTRODUCTION

The spin Hall effect (SHE)—the generation of transverse spin current in response to a longitudinal electrical injection in nonmagnetic heavy metals (N) with strong spin-orbit coupling (SOC)—has attracted extensive research interest [1–4]. In ferromagnetic metals (F) with SOC, spin currents are induced perpendicular to both the electrical injection and the magnetization directions due to the related anomalous Hall effect (AHE) [5–7]. In this paper, we focus on the thermoelectric counterparts of the SHE and AHE, i.e., the thermally induced spin currents generated by the spin Nernst effect (SNE) and anomalous Nernst effect (ANE).

The conversion of heat currents into spin currents in N with SOC such as Pt and W via SNE has been investigated theoretically and experimentally recently [8–11]. The SNE describes a transverse pure spin current driven by a longitudinal temperature gradient (i.e., heat current), which shares a geometrical analogy with the SHE. Similarly, applying a thermal gradient in F generates an electric field mutually perpendicular to both the heat flow and the magnetization, giving rise to the so-called ANE [12–14]. The measured output which is usually used to characterize the SNE and ANE is the thermally induced electric voltage induced via the inverse spin Hall effect (ISHE) [i.e., thermally driven spin Hall magnetoresistance (TSMR) effect] in F/N heterostructures [8,10,13,15].

In this work, we consider the SNE and ANE on equal footing in F/N heterostructures. Under an in-plane temperature gradient, spin currents are thermally excited in F due to the ANE and in N due to the SNE simultaneously, which can be converted into electric voltages in N via the ISHE (i.e., TSMR voltages) or spin torques on the adjacent F layers. The motivation of this work is to capture and characterize the interplay of SNE and ANE in F/N heterostructures via a single measurement setup, and study how these translate into their different signature outputs, from which the underlying physics could be addressed. We present a drift-diffusion transport model to describe the SNE and ANE-induced spin currents, and evaluate analytically as well as numerically the resulting electric TSMR voltage and ferromagnetic resonance (FMR) spectrum as two signature outputs. In a F/N bilayer, the spin currents manifest themselves as TSMR voltages in the N layer. In addition to the expected local SNE contribution in the N, our analytical results show that ANE in the adjacent F layer also has a nonlocal or mixing contribution to the TSMR output, which represents the interplay of these two thermal effects and gives rise to the magnetization dependence of the signal measured in the N. Interestingly, the SNE and ANE contributions to the TSMR output are found to contribute additively (in opposition to one another) for the transverse (longitudinal) component of the TSMR voltage. This anisotropic response allows a possible means to differentiate the individual contributions of SNE and ANE, and spin polarization parameters to be extracted. Additionally we consider a F1/N/F2 trilayer and derive the FMR output spectrum of the F2 layer due to the combined effect of SNE in the N and ANE in the F1.

*e0021580@u.nus.edu
†elembaj@nus.edu.sg

 

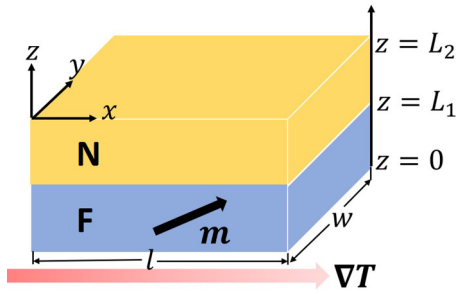


FIG. 1. Schematic diagram of the F/N structure in this work. The direction of $\boldsymbol{m}$ in the F layer can point in any arbitrary direction. The in-plane temperature gradient $\nabla T$ along the $x$ direction is applied to the whole stack, which generates spin currents in F with ANE and N with SNE simultaneously. Here, we focus on the perpendicular-to-plane transport along the $z$ direction.

Unlike the anisotropic response of the TSMR output, the SNE and ANE contribute additively to the magnitude and linewidth of the FMR. By comparing these two thermoelectric outputs in the F/N and F1/N/F2 heterostructures, it is found that the TSMR voltage signal in F/N bilayers can potentially provide a more sensitive detection of the interplay of SNE and ANE.

This paper is organized as follows. In Sec. II A, we present the basic expressions of spin current densities generated in the N due to SNE and in the F due to ANE, separately. They serve as the framework for further derivations of the TSMR and FMR output signals based on the F/N heterostructures in Secs. II B and II C, respectively, which form the main results of the paper. A conclusion is presented in Sec. III.

## II. THEORY AND ANALYSIS

### A. Spin currents in the F and the N layers

A drift-diffusion treatment is utilized to describe spin transports in the F/N structure as schematically shown in Fig. 1, where the applied in-plane temperature gradient is along the $x$ direction (i.e., $\nabla T = \hat{\boldsymbol{x}}\partial_x T$), and we focus on the perpendicular-to-plane transport along the $z$ direction.

The SNE describes a generation of transverse pure spin current from $\partial_x T$ in N with strong SOC. Similar to the geometrical symmetry of SHE [16], the pure spin current density along the $z$ direction in the N is described by

$$\boldsymbol{j}_{sz,\mathrm{N}} = -\frac{\sigma_\mathrm{N}}{e}\partial_z \boldsymbol{\mu}_{s,\mathrm{N}} + j_{\mathrm{SNE}}\hat{\boldsymbol{y}}, \tag{1}$$

which consists of the diffusive and SNE drift contributions, respectively. In the above equation, the vector direction refers to the spin orientation, while the current flow is along the $z$ direction. The first term is the usual diffusive contribution given by the spatial derivative of the spin accumulation $\boldsymbol{\mu}_s$, which satisfies the general drift-diffusion equation $\frac{\partial^2 \boldsymbol{\mu}_s}{\partial z^2} = \frac{\boldsymbol{\mu}_s}{\lambda^2}$ with $\lambda$ the corresponding spin diffusion length [17]. $\sigma_\mathrm{N}$ is the conductivity of N and $e = |e|$ is the electron charge. The second term is the drift contribution $j_{\mathrm{SNE}} = \sigma_\mathrm{N} N_{\mathrm{SNE}} \partial_x T$ due to the spin Nernst current generated directly by the SNE, where $N_{\mathrm{SNE}}$ is the spin Nernst coefficient denoting the heat-spin conversion efficiency. Note that spin quantities in N (i.e., $\boldsymbol{\mu}_{s,\mathrm{N}}$ and $\boldsymbol{j}_{sz,\mathrm{N}}$) have three polarization components since the spin polarization direction within the N is arbitrary and would have to be determined by applying the boundary conditions [16]. However, $\boldsymbol{j}_{\mathrm{SNE}}$ is purely composed of the $y$ component (i.e., $\hat{\boldsymbol{y}}$) due to the SNE symmetry [8].

We now consider the spin current in the F layer. A strong SOC in the F can generate a spin current under a temperature gradient, i.e., the ANE which can be considered as the thermoelectric counterpart of AHE. An electric field mutually perpendicular to both the heat flow and the magnetization is generated, i.e., the spins are polarized along the local magnetization direction (i.e., $\boldsymbol{m}$), and flowing in the $\boldsymbol{m} \times \nabla T$ direction. Note that the spin current is generated with the electric current as a result of the spin-dependent transport properties in F, i.e., the electric current is spin polarized. The electric and spin current densities in F with ANE are described by [18]

$$\mathbf{j}_{c,\mathrm{F}} = \frac{\sigma_\mathrm{F}}{e}\nabla\mu_{c,\mathrm{F}} + \beta_\mathrm{F}\frac{\sigma_\mathrm{F}}{e}\nabla\mu_{s,\mathrm{F}} + \sigma_\mathrm{F} N_{\mathrm{ANE}}(\boldsymbol{m} \times \nabla T) \tag{2}$$

and

$$\mathbf{j}_{s,\mathrm{F}} = -\frac{\sigma_\mathrm{F}}{e}\nabla\mu_{s,\mathrm{F}} - \beta_\mathrm{F}\frac{\sigma_\mathrm{F}}{e}\nabla\mu_{c,\mathrm{F}} - \sigma_\mathrm{F} p N_{\mathrm{ANE}}(\boldsymbol{m} \times \nabla T), \tag{3}$$

where the first two terms denote diffusion and the third term is the ANE drift contribution. $\sigma_\mathrm{F}$ is the conductivity of F whose spin polarization is described by $\beta_\mathrm{F} = \frac{\sigma_{\mathrm{F},\uparrow} - \sigma_{\mathrm{F},\downarrow}}{\sigma_\mathrm{F}}$ with $\sigma_\mathrm{F} = \sigma_{\mathrm{F},\uparrow} + \sigma_{\mathrm{F},\downarrow}$ [17]. Here $\uparrow(\downarrow)$ denotes the longitudinal polarization direction parallel (antiparallel) to $\boldsymbol{m}$ in the F. In Eqs. (2) and (3), the direction of the vectors refers to the direction of the current flow. Compared with spin accumulation $\mu_s = \frac{\mu_\uparrow - \mu_\downarrow}{2}$, charge accumulation is defined as $\mu_c = \frac{\mu_\uparrow + \mu_\downarrow}{2}$. As for the ANE contribution along $\boldsymbol{m} \times \nabla T$, $N_{\mathrm{ANE}}$ is the corresponding anomalous Nernst coefficient with a polarization $p = \frac{N_{\mathrm{ANE},\uparrow} - N_{\mathrm{ANE},\downarrow}}{N_{\mathrm{ANE},\uparrow} + N_{\mathrm{ANE},\downarrow}}$ [18]. Note the (average) anomalous Nernst coefficient is given by $N_{\mathrm{ANE}} = \frac{\sigma_{\mathrm{F},\uparrow} N_{\mathrm{ANE},\uparrow} + \sigma_{\mathrm{F},\downarrow} N_{\mathrm{ANE},\downarrow}}{\sigma_\mathrm{F}}$ [18]. Combining Eqs. (2) and (3) with the open circuit boundary conditions along the $z$ direction, the spin current density flows along the $z$ direction (i.e., the $z$ component of $\mathbf{j}_{s,\mathrm{F}}$) is given by

$$j_{sz,\mathrm{F}} = -\left(1 - \beta_\mathrm{F}^2\right)\frac{\sigma_\mathrm{F}}{e}\partial_z \mu_{s,\mathrm{F}} + j_{\mathrm{ANE}}, \tag{4}$$

which possesses a similar form to that of the spin current density in N with SNE given by Eq. (1). However, unlike in N where the spin current and accumulation possess arbitrary polarization direction, the spin polarization of the spin components in F are considered to be aligned along the local magnetization direction (e.g., $\boldsymbol{j}_{sz,\mathrm{F}} = j_{sz,\mathrm{F}}\boldsymbol{m}$) [6,19]. $j_{\mathrm{ANE}}$ is the spin anomalous Nernst current density generated directly by the ANE and can be expressed as

$$j_{\mathrm{ANE}} = m_y(p - \beta_\mathrm{F})\sigma_\mathrm{F} N_{\mathrm{ANE}} \partial_x T, \tag{5}$$

where $m_y$ is the $y$ component of $\boldsymbol{m}$, indicating that ANE contributes to the spin transport flows along the $z$ direction only when $\boldsymbol{m}$ has a nonzero $y$ component.

### B. TSMR voltage in F/N bilayer

In a bilayer consisting of an insulating F and a metallic N with SOC, the simultaneous action of SHE and ISHE induces the spin Hall magnetoresistance (SMR) [16,20]. Similarly, in the metallic F/N bilayer, the combined effect of SNE and ANE results in a thermal voltage via the ISHE, along and transverse to the applied temperature gradient. This thermally driven spin Hall magnetoresistance (TSMR) is derived and analyzed in this section.

Here we introduce the interfacial spin current density notation $\mathbf{Q}$ at the F/N interface, which is defined as being injected from F to N. With the spin current densities given by Eqs. (1) and (4), we apply the following boundary conditions for the F/N bilayer (Fig. 1): (i) at both terminals in the $z$ direction, the spin current densities vanish, i.e., $j_{sz,\mathrm{F}}(0)=0$ and $\boldsymbol{j}_{sz,\mathrm{N}}(L_2)=\mathbf{0}$; (ii) at the F/N interface, we have $\boldsymbol{j}_{sz,\mathrm{N}}(L_1)=\mathbf{Q}$ and $j_{sz,\mathrm{F}}(L_1)=\boldsymbol{m}\cdot\mathbf{Q}$. With the above boundary conditions, by solving the general drift-diffusion equation (i.e., $\frac{\partial^2\boldsymbol{\mu}_s}{\partial z^2}=\frac{\boldsymbol{\mu}_s}{\lambda^2}$) the spin accumulations in F/N can be expressed in terms of $\mathbf{Q}$ as

$$\mu_{s,\mathrm{F}}=-\frac{e}{g_\mathrm{F}}\mathrm{csch}\left(\frac{t_\mathrm{F}}{\lambda_\mathrm{F}}\right)\left\{j_\mathrm{ANE}\left[\cosh\left(\frac{t_\mathrm{F}-z}{\lambda_\mathrm{F}}\right)-\cosh\left(\frac{z}{\lambda_\mathrm{F}}\right)\right]+\cosh\left(\frac{z}{\lambda_\mathrm{F}}\right)\boldsymbol{m}\cdot\mathbf{Q}\right\} \tag{6}$$

and

$$\boldsymbol{\mu}_{s,\mathrm{N}}=\frac{e}{g_\mathrm{N}}\mathrm{csch}\left(\frac{t_\mathrm{N}}{\lambda_\mathrm{N}}\right)\left\{j_\mathrm{SNE}\left[\cosh\left(\frac{t_\mathrm{N}-z}{\lambda_\mathrm{N}}\right)-\cosh\left(\frac{t_\mathrm{F}+t_\mathrm{N}-z}{\lambda_\mathrm{N}}\right)\right]\hat{\boldsymbol{y}}+\cosh\left(\frac{t_\mathrm{F}+t_\mathrm{N}-z}{\lambda_\mathrm{N}}\right)\mathbf{Q}\right\}, \tag{7}$$

where $g_\mathrm{F}=\frac{(1-\beta_\mathrm{F}^2)\sigma_\mathrm{F}}{\lambda_\mathrm{F}}$ and $g_\mathrm{N}=\frac{\sigma_\mathrm{N}}{\lambda_\mathrm{N}}$ are introduced. $t_{\mathrm{F(N)}}$ represents the thickness of the F(N) layer. On the other hand, the interfacial spin current density $\mathbf{Q}$ is also governed by the various interfacial conductances at the F/N interface ($z=L_1$) [7,21–24]:

$$e\mathbf{Q}=G_0[\mu_{s,\mathrm{F}}(L_1)-\boldsymbol{m}\cdot\boldsymbol{\mu}_{s,\mathrm{N}}(L_1)]\boldsymbol{m}+2G_r\boldsymbol{m}\times[\boldsymbol{m}\times\boldsymbol{\mu}_{s,\mathrm{N}}(L_1)]+2G_i[\boldsymbol{m}\times\boldsymbol{\mu}_{s,\mathrm{N}}(L_1)], \tag{8}$$

where $G_0=\frac{4G_\uparrow G_\downarrow}{G_\uparrow+G_\downarrow}$. $G_\uparrow$ and $G_\downarrow$ are the interfacial conductances of up spin and down spin. $G_r$ and $G_i$ represent the real and imaginary part of the mixing conductance, respectively. Here we apply $G_i=0$ since it is approximately an order of magnitude smaller than $G_r$ for simplicity [25]. Note that in order to obtain Eq. (8), the charge accumulation has been eliminated after considering the open-circuit boundary condition at the interface [6,7]. By substituting Eqs. (6) and (7) into Eq. (8), the full solution for the interfacial spin current density $\mathbf{Q}$ can be obtained, which yields a rather lengthy expression. Hence, for brevity, we express the solution of $\mathbf{Q}$ in terms of the effective conductances (i.e., $g_0^*$, $g_1^*$, and $g_2^*$), i.e.,

$$e\mathbf{Q}=g_0^*\left(\mu_\mathrm{ANE}^0+m_y\mu_\mathrm{SNE}^0\right)\boldsymbol{m}+\mu_\mathrm{SNE}^0[g_1^*\boldsymbol{m}\times(\boldsymbol{m}\times\hat{\boldsymbol{y}})+g_2^*\boldsymbol{m}\times\hat{\boldsymbol{y}}], \tag{9}$$

where $\mu_\mathrm{ANE}^0=\frac{e}{g_\mathrm{F}}\tanh(\frac{t_\mathrm{F}}{2\lambda_\mathrm{F}})j_\mathrm{ANE}$ and $\mu_\mathrm{SNE}^0=\frac{e}{g_\mathrm{N}}\tanh(\frac{t_\mathrm{N}}{2\lambda_\mathrm{N}})j_\mathrm{SNE}$. $\mu_{\mathrm{ANE(SNE)}}^0$ is the ANE(SNE)-generated spin accumulation at the F/N interface in the absence of spin transfer, i.e., when there is zero interfacial mixing conductance [16]. The explicit expressions of these effective conductances are given by

$$\frac{1}{g_0^*}=\frac{1}{g_\mathrm{F}\tanh(t_\mathrm{F}/\lambda_\mathrm{F})}+\frac{1}{G_0}+\frac{1}{g_\mathrm{N}\tanh(t_\mathrm{N}/\lambda_\mathrm{N})} \tag{10}$$

and

$$\frac{1}{g_1^*}=\frac{1}{g_\mathrm{N}\tanh(t_\mathrm{N}/\lambda_\mathrm{N})}+\frac{1}{2G_r}, \tag{11}$$

while the third $g_2^*$ is proportional to $G_i$, and hence zero due to our assumption that $G_i=0$. Equation (9) indicates that both ANE in F and SNE in N contribute to the longitudinal component (i.e., polarized along $\boldsymbol{m}$) of the interfacial spin current density at the F/N interface (i.e., $\mathbf{Q}$) through $g_0^*$, while only SNE in N contributes to the transverse (i.e., polarized perpendicular to $\boldsymbol{m}$) components, which are governed by $g_1^*$ and $g_2^*$. This is understandable since only the longitudinal spin component along the local magnetization direction $\boldsymbol{m}$ in F is considered, i.e., ANE in F only affects the longitudinal spin current density at the F/N interface. Consequently, the final expressions of the spin accumulations in F and N can be obtained by substituting Eq. (9) into Eqs. (6) and (7).

Having solved for the spin accumulation, we now evaluate the ISHE voltage as the output of the SNE and ANE in the F/N bilayer. In the N with SOC, the ISHE converts the diffusion spin current flowing along the $z$ direction [i.e., $\boldsymbol{j}_{sz,\mathrm{N}}$ given by Eq. (1)] to an electric current in the $x$-$y$ plane. The ISHE-generated longitudinal (along the thermal gradient direction, i.e., $\hat{\boldsymbol{x}}$) and transverse (along $\hat{\boldsymbol{y}}$) electric currents are described by

$$j_{cx,\mathrm{N}}=-\theta_\mathrm{SHE}\frac{\sigma_\mathrm{N}}{e}\partial_z\mu_{s,\mathrm{N}}^y+j_\mathrm{SE} \tag{12}$$

and

$$j_{cy,\mathrm{N}}=\theta_\mathrm{SHE}\frac{\sigma_\mathrm{N}}{e}\partial_z\mu_{s,\mathrm{N}}^x, \tag{13}$$

where $j_\mathrm{SE}=-\sigma_\mathrm{N}S_\mathrm{N}\partial_x T$ is the normal Seebeck effect in N under the in-plane temperature gradient $\partial_x T$ with $S_\mathrm{N}$ the corresponding Seebeck coefficient. $\theta_\mathrm{SHE}$ is the spin Hall angle describing the spin-charge conversion via the ISHE. Here $\mu_{s,\mathrm{N}}^{x(y)}$ represents the $x(y)$ polarization component of $\boldsymbol{\mu}_{s,\mathrm{N}}$. Note that $j_{cz,\mathrm{N}}=0$ since the open circuit configuration is applied. Based on the generated electric currents, the longitudinal and transverse voltages can be calculated by averaging the electric currents over the film thickness as $V_\mathrm{thermal}^\mathrm{L}/l=\frac{1}{t_\mathrm{N}}\int_{L_1}^{L_2}\frac{j_{cx,\mathrm{N}}}{\sigma_\mathrm{N}}dz$ and $V_\mathrm{thermal}^\mathrm{T}/w=\frac{1}{t_\mathrm{N}}\int_{L_1}^{L_2}\frac{j_{cy,\mathrm{N}}}{\sigma_\mathrm{N}}dz$ respectively, where $l$ and $w$ denote the sample length and width, respectively. Substituting the full expression for the spin accumulation which we have solved for earlier, the detected thermal voltages can be expressed as

$$\frac{V_\mathrm{thermal}^\mathrm{L}}{l}=-\left[S_\mathrm{N}+\Delta S_{\mathrm{SNE},1}^\mathrm{L}+\left(\Delta S_\mathrm{ANE}^\mathrm{L}+\Delta S_{\mathrm{SNE},2}^\mathrm{L}\right)m_y^2+\Delta S_{\mathrm{SNE},3}^\mathrm{L}\left(1-m_y^2\right)\right]\partial_x T \tag{14}$$

and

$$\frac{V^{\mathrm{T}}_{\mathrm{thermal}}}{w} = \left[\left(\Delta S^{\mathrm{T}}_{\mathrm{ANE}} + \Delta S^{\mathrm{T}}_{\mathrm{SNE},1}\right) m_x m_y + \Delta S^{\mathrm{T}}_{\mathrm{SNE},2} m_z\right] \partial_x T. \tag{15}$$

Here several effective Seebeck coefficients are introduced with

$$\Delta S^{\mathrm{L}}_{\mathrm{SNE},1} = \frac{2\lambda_{\mathrm{N}}}{t_{\mathrm{N}}} \tanh\left(\frac{t_{\mathrm{N}}}{2\lambda_{\mathrm{N}}}\right)(\theta_{\mathrm{SHE}} N_{\mathrm{SNE}}), \tag{16}$$

$$\Delta S^{\mathrm{L}}_{\mathrm{ANE}} = \frac{\beta_{\mathrm{F}} - p}{1-\beta_{\mathrm{F}}^2} \frac{\lambda_{\mathrm{F}}}{t_{\mathrm{N}}} \frac{g_0^*}{g_{\mathrm{N}}} \tanh\left(\frac{t_{\mathrm{F}}}{2\lambda_{\mathrm{F}}}\right) \tanh\left(\frac{t_{\mathrm{N}}}{2\lambda_{\mathrm{N}}}\right)(\theta_{\mathrm{SHE}} N_{\mathrm{ANE}}), \tag{17}$$

$$\Delta S^{\mathrm{L}}_{\mathrm{SNE},2} = -\frac{\lambda_{\mathrm{N}}}{t_{\mathrm{N}}} \frac{g_0^*}{g_{\mathrm{N}}} \tanh^2\left(\frac{t_{\mathrm{N}}}{2\lambda_{\mathrm{N}}}\right)(\theta_{\mathrm{SHE}} N_{\mathrm{SNE}}), \tag{18}$$

$$\Delta S^{\mathrm{L}}_{\mathrm{SNE},3} = \frac{\lambda_{\mathrm{N}}}{t_{\mathrm{N}}} \frac{g_1^*}{g_{\mathrm{N}}} \tanh^2\left(\frac{t_{\mathrm{N}}}{2\lambda_{\mathrm{N}}}\right)(\theta_{\mathrm{SHE}} N_{\mathrm{SNE}}), \tag{19}$$

$$\Delta S^{\mathrm{T}}_{\mathrm{ANE}} = \Delta S^{\mathrm{L}}_{\mathrm{ANE}}, \tag{20}$$

$$\Delta S^{\mathrm{T}}_{\mathrm{SNE},1} = -\frac{1}{1-\beta_{\mathrm{F}}^2} \frac{\lambda_{\mathrm{F}}}{t_{\mathrm{N}}} \frac{g_{\mathrm{F}}(g_0^* + g_1^*)}{g_{\mathrm{N}}^2} \tanh^2\left(\frac{t_{\mathrm{N}}}{2\lambda_{\mathrm{N}}}\right)(\theta_{\mathrm{SHE}} N_{\mathrm{SNE}}), \tag{21}$$

and

$$\Delta S^{\mathrm{T}}_{\mathrm{SNE},2} = \frac{\lambda_{\mathrm{N}}}{t_{\mathrm{N}}} \frac{g_2^*}{g_{\mathrm{N}}} \tanh^2\left(\frac{t_{\mathrm{N}}}{2\lambda_{\mathrm{N}}}\right)(\theta_{\mathrm{SHE}} N_{\mathrm{SNE}}), \tag{22}$$

which can be referred to as the thermal analogs of spin Hall magnetoresistance, i.e., TSMR. In Eqs. (14)–(22), the superscripts L and T denote the longitudinal (i.e., along the current direction or $x$ direction) and transverse (along the $y$ direction) contributions to the TSMR voltages, respectively. The physics in operation is as follows: The spin currents are generated in the F due to ANE and N due to SNE. These respectively undergo partial transmission and reflection at the F/N interface. In the N, the reflected SNE-induced spin current is transferred to the charge current by the ISHE, which in turn generates the TSMR voltage. In the derived expression of $V^{\mathrm{L}}_{\mathrm{thermal}}$ [i.e., Eq. (14)], there are three effective Seebeck coefficients originating from SNE (i.e., $\Delta S^{\mathrm{L}}_{\mathrm{SNE},1-3}$ with respect to $\theta_{\mathrm{SHE}} N_{\mathrm{SNE}}$), which correspond to three different dependencies on the magnetization $\boldsymbol{m}$. Similarly, for the transverse voltage $V^{\mathrm{T}}_{\mathrm{thermal}}$ in Eq. (15), there are two SNE-induced effective Seebeck coefficients (i.e., $\Delta S^{\mathrm{T}}_{\mathrm{SNE},1-2}$ with respect to $\theta_{\mathrm{SHE}} N_{\mathrm{SNE}}$) corresponding to two different $\boldsymbol{m}$ dependencies. Since the TSMR voltages $V^{\mathrm{L}}_{\mathrm{thermal}}$ and $V^{\mathrm{T}}_{\mathrm{thermal}}$ arise in the N layer due to the ISHE, where the SNE is also occurring, the terms corresponding to $\Delta S^{\mathrm{L}}_{\mathrm{SNE},1-3}$ and $\Delta S^{\mathrm{T}}_{\mathrm{SNE},1-2}$ represent the local effects. Meanwhile, the ANE-induced spin current in the F which is transmitted into the N undergoes conversion to a charge current via the ISHE, yielding another contribution to the TSMR voltage. This physical process is captured by the derived effective Seebeck coefficients [i.e., $\Delta S^{\mathrm{L}}_{\mathrm{ANE}}$ and $\Delta S^{\mathrm{T}}_{\mathrm{ANE}}$ ] with respect to $\theta_{\mathrm{SHE}} N_{\mathrm{ANE}}$, and represents the mixing (nonlocal) contribution to the TSMR voltage induced by the ANE in the adjacent F. In Eqs. (14) and (15), $\Delta S^{\mathrm{L}}_{\mathrm{ANE}}$ and $\Delta S^{\mathrm{T}}_{\mathrm{ANE}}$ depend on $m_y^2$ and $m_x m_y$, respectively. These mixing contributions allow the TSMR output signal to be modulated by varying the magnetization direction of the F layer, and thereby manifesting the interplay of SNE and ANE.

The TSMR measurement is widely used to investigate thermally induced spin transport experimentally [8,10,13,15]. For numerical calculations, we assume a NiFe(F)/Pt(N) bilayer structure. It has been experimentally investigated that Pt possesses SNE with spin Nernst coefficient $N_{\mathrm{SNE}} = 4.73\,\mu\mathrm{V/K}$ [11]. As for ANE, we utilize a comparable anomalous Nernst coefficient of $N_{\mathrm{ANE}} = 4\,\mu\mathrm{V/K}$, which is on the same order of magnitude as experimental measured values [26]. Therefore, we are considering SNE and ANE with comparable Nernst coefficients. The other material parameters are (i) in the F [27,28]: $\rho_{\mathrm{F}} = 241\,\Omega\,\mathrm{nm}$, $\lambda_{\mathrm{F}} = 5.5\,\mathrm{nm}$, $\beta_{\mathrm{F}} = 0.7$, and $p = 3$; (ii) in the N [8,29]: $\rho_{\mathrm{N}} = 397\,\Omega\,\mathrm{nm}$, $\lambda_{\mathrm{N}} = 1.5\,\mathrm{nm}$, and $\theta_{\mathrm{SHE}} = 0.11$. The thicknesses are assumed to be $t_{\mathrm{F}} = 10\,\mathrm{nm}$ and $t_{\mathrm{N}} = 4\,\mathrm{nm}$. For the longitudinal interfacial conductances, we use the representative values assumed previously [23,24] since there are no available experimental measurements, i.e., $G_{\uparrow} = 0.42 \times 10^{15}\,\Omega^{-1}\,\mathrm{m}^{-2}$ and $G_{\downarrow} = 0.36 \times 10^{15}\,\Omega^{-1}\,\mathrm{m}^{-2}$. On the other hand, we utilize the interfacial mixing conductance $G_r = 0.5 \times 10^{15}\,\Omega^{-1}\,\mathrm{m}^{-2}$, which is a representative experimental value for the general F/Pt interfaces [30,31]. Based on an SNE experiment reported in Ref. [8], we utilize a longitudinal temperature difference $\Delta T = 18\,\mathrm{K}$ over a sample size of $l = 3\,\mathrm{mm}$, which corresponds to a thermal gradient of $\partial_x T = 6 \times 10^{-6}\,\mathrm{K/nm}$. Based on these parameters, we compute the angular and layer thickness dependence of the longitudinal and transverse TSMR voltages.

Typically in experiments, the angular dependence of the SMR voltage is measured [20,32,33], in which an external saturation magnetic field is applied to align $\boldsymbol{m}$ along various directions. Consider that the magnetization $\boldsymbol{m}$ of F is rotated in three different rotation planes [i.e., $x$-$y$ plane with $\boldsymbol{m} = (\cos\alpha, \sin\alpha, 0)$, $y$-$z$ plane with $\boldsymbol{m} = (0, \cos\beta, \sin\beta)$, and $z$-$x$ plane with $\boldsymbol{m} = (\cos\gamma, 0, \sin\gamma)$ ]; we plot the angular dependence of TSMR voltages in Fig. 2 for three cases: (i) only SNE contributes, i.e., $N_{\mathrm{ANE}} = 0$ in the F, (ii) only ANE contributes, i.e., $N_{\mathrm{SNE}} = 0$ in the N, and (iii) both SNE and ANE contribute. It can be seen that $V^{\mathrm{L}}_{\mathrm{thermal}}$ gives a $\sin^2\alpha$ (or $\cos^2\beta$) dependence in Fig. 2(a) [or Fig. 2(b)] and $V^{\mathrm{T}}_{\mathrm{thermal}}$ exhibits a $\cos\alpha\sin\alpha$ dependence in Fig. 2(d), which correspond to the $m_y^2$ terms in Eq. (14) and the $m_x m_y$ term in Eq. (15), respectively. These angular dependencies of TSMR are in agreement with experimentally measured angular dependence of SMR [20,32,33], in which the output voltage is induced by the SHE. Similarly, $V^{\mathrm{L}}_{\mathrm{thermal}}$ remains constant when $\boldsymbol{m}$ rotates in the $z$-$x$ plane, as shown in Fig. 2(c), since $V^{\mathrm{L}}$ has dependence only on $m_y^2$ as given by Eq. (14). Note that $V^{\mathrm{T}}_{\mathrm{thermal}}$ becomes zero when $\boldsymbol{m}$ rotates in the $y$-$z$ ($z$-$x$) planes due to its $m_x m_y$ dependence [Eq. (15)] with $g_2^* = 0$. Interestingly, SNE and ANE give voltage contributions of opposite signs for $V^{\mathrm{L}}_{\mathrm{thermal}}$, i.e., $V^{\mathrm{L}}_{\mathrm{thermal}}$ decreases when both SNE and ANE exist. However, $V^{\mathrm{T}}_{\mathrm{thermal}}$ is enhanced when both SNE and ANE contribute, and this difference in trend can provide useful information of the spin-dependent polarization parameters in the F (i.e., $\beta_{\mathrm{F}}$ and $p$) via comparison of Eqs. (20) with (21). Note both the sign and magnitude of the TSMR voltage are dependent on the two key polarization parameters ($p$ and $\beta_{\mathrm{F}}$), e.g., $\Delta S^{\mathrm{L}}_{\mathrm{ANE}}$ is determined by the factor $\frac{\beta_{\mathrm{F}} - p}{1-\beta_{\mathrm{F}}^2}$ [see Eq. (17)]. This anisotropic response

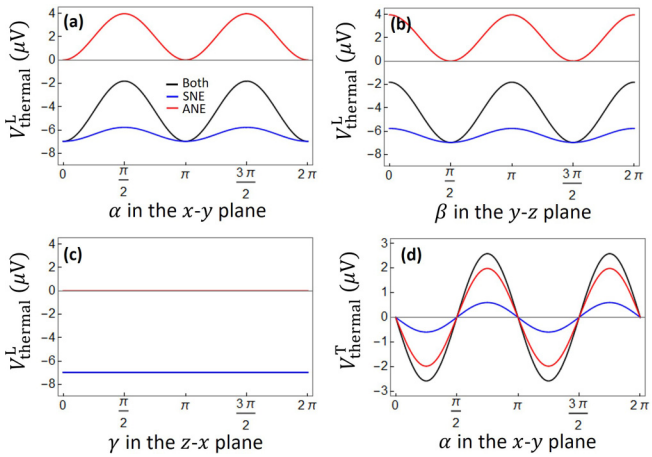


FIG. 2. Angular dependence of TSMR voltages. The longitudinal TSMR voltage $V^{\mathrm{L}}_{\mathrm{thermal}}$ is depicted for three magnetization rotation geometries: (a) $\boldsymbol{m}$ is rotated in the $x$-$y$ plane with $\boldsymbol{m} = (\cos\alpha, \sin\alpha, 0)$, (b) $\boldsymbol{m}$ is rotated in the $y$-$z$ plane with $\boldsymbol{m} = (0, \cos\beta, \sin\beta)$, and (c) $\boldsymbol{m}$ is rotated in the $z$-$x$ plane with $\boldsymbol{m} = (\cos\gamma, 0, \sin\gamma)$. The transverse TSMR voltage $V^{\mathrm{T}}_{\mathrm{thermal}}$ is plotted when $\boldsymbol{m}$ is rotated in the $x$-$y$ plane with $\boldsymbol{m} = (\cos\alpha, \sin\alpha, 0)$ in (d). The blue, red, and black lines represent voltage contributions from only SNE, only ANE, and both of them, respectively. Here we use $l = w = 3$ mm and $\Delta T = 18$ K. Note that the constant Seebeck voltage contribution [i.e., the first term in Eq. (14)] is subtracted for $V^{\mathrm{L}}_{\mathrm{thermal}}$.

also allows a possible means to differentiate the individual contributions of SNE and ANE. The contribution difference between SNE and ANE can also be seen in the TSMR voltage plotting of layer thickness dependence (i.e., Fig. 3). In addition, a $V^{\mathrm{T}}_{\mathrm{thermal}}$ maximum can be obtained by tuning $t_{\mathrm{N}}$ where both SNE and ANE contribute additively, as shown in Fig. 3(c). This maximum is achieved at $t_{\mathrm{N}}$ approaches the

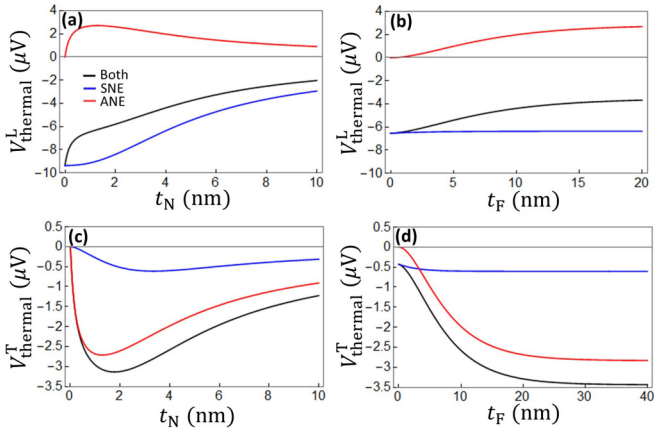


FIG. 3. Layer thickness dependence of TSMR voltages when $\boldsymbol{m} = (\frac{1}{\sqrt{2}}, \frac{1}{\sqrt{2}}, 0)$. $V^{\mathrm{L}}_{\mathrm{thermal}}$ is depicted as a function of $t_{\mathrm{N}}$ in (a) and $t_{\mathrm{F}}$ in (b), and $V^{\mathrm{T}}_{\mathrm{thermal}}$ is depicted as a function of $t_{\mathrm{N}}$ in (c) and $t_{\mathrm{F}}$ in (d). $t_{\mathrm{F}} = 10$ nm is fixed in (a) and (c), and $t_{\mathrm{N}} = 4$ nm in (b) and (d). The blue, red, and black lines represent voltage contributions from only SNE, only ANE, and both of them, respectively. Here we use $l = w = 3$ mm and $\Delta T = 18$ K. Note that the constant Seebeck voltage contribution [i.e., the first term in Eq. (14)] is subtracted for $V^{\mathrm{L}}_{\mathrm{thermal}}$.

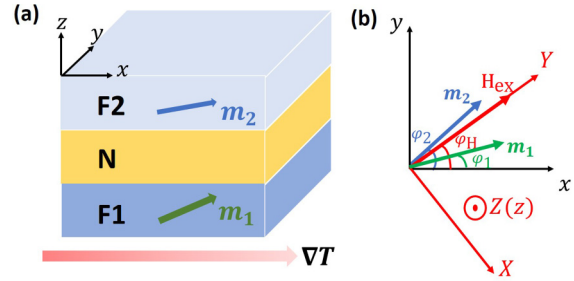


FIG. 4. (a) Schematic diagram of the F1/N/F2 structure. The in-plane temperature gradient $\nabla T$ along the $x$ direction is applied to the whole stack, which generates spin currents in F1 with ANE and N with SNE, resulting in spin torques exerted on the free F2. (b) The $XYZ$ coordinate system used in the FMR analysis, where the static external magnetic field $\mathrm{H_{ex}}$ is applied along the $Y$ direction. Here we consider both $\boldsymbol{m}_1$ and $\boldsymbol{m}_2$ are in-plane magnetized.

spin diffusion length $\lambda_{\mathrm{N}} = 1.5$ nm, which follows the usual trend in spin drift-diffusive transport [3,34,35]. However, as $t_{\mathrm{F}}$ increases, the TSMR voltage increases in a monotonous fashion and then saturates, which is understandable as a larger ANE contribution from F would result with larger $t_{\mathrm{F}}$ but this begins to saturate as $t_{\mathrm{F}}$ exceeds $\lambda_{\mathrm{F}}$.

For the above numerical calculations, the applied thermal gradient of $\partial_x T = 6 \times 10^{-6}$ K/nm [8] gives the TSMR output in the order of several microvolts, which is a readily measurable voltage. From Eqs. (14) and (15), it can be seen that the longitudinal (transverse) TSMR voltage is proportional to the sample length (width). Based on the material parameters used here, the TSMR voltage measurement has the advantage to clearly detect the SNE and ANE with minor thermal injection as low as $\partial_x T \sim 10^{-6}$ K/nm by enhancing the sample length to the order of 1 mm. On the other hand, when the sample lateral width is on the order of several microns, a larger thermal gradient of $\partial_x T \sim 10^{-3}$ K/nm is required to generate measurable TSMR voltages in the microvolt range. This value is still achievable and much smaller than the largest thermal gradient of 0.1 K/nm in proposed experimental setups [36].

As for the interfacial conductance dependence of the TSMR voltages, by considering the boundary conditions at the F/N interface [i.e., Eq. (8)], it is straightforward to see that the interfacial spin current densities increases with interfacial conductance values. However, numerically it was found that the TSMR voltage has only a weak dependence on the interfacial conductance (not shown here). This dependence can be neglected since the interfacial conductance for different F/N interfaces generally fall within the same order of magnitude of $\sim 10^{15}\ \Omega^{-1}\,\mathrm{m}^{-2}$ [30,31,37,38].

### C. FMR analysis of spin torques in F1/N/F2 trilayer

In this section, we consider an alternative method of quantifying the ANE and SNE involving a F1/N/F2 trilayer structure (Fig. 4). As in the bilayer structure, the ANE-induced spin current in the F1 and SNE-induced spin current in the N undergoes partial reflection and transmission at both the F1/N and N/F2 interfaces. The spin current transmitted into the free F2 layer exerts spin torques on the local magnetization. $\boldsymbol{m}_{1(2)}$ denotes the unit magnetization vector in F1(F2).

Similar to the previous section, we introduce the interfacial spin current density, i.e., $\mathbf{Q}_{1(2)}$ at the F1(F2)/N interface, which is defined as being injected from F1(F2) to N. The resulting spin torque acting on the free F2 is given by

$$\boldsymbol{T} = -\boldsymbol{m}_2 \times (\mathbf{Q}_2 \times \boldsymbol{m}_2) = \boldsymbol{m}_2 \times (\boldsymbol{m}_2 \times \mathbf{Q}_2). \tag{23}$$

The minus sign in Eq. (23) denotes the fact that $\mathbf{Q}_2$ is being injected from F2 to N, i.e., along the $-z$ direction. Both $\mathbf{Q}_1$ and $\mathbf{Q}_2$ are related to their different corresponding spin accumulations and magnetizations at the F1/N ($z = L_1$) and F2/N ($z = L_2$) interfaces, respectively, in the same form as described by Eq. (8), and the same interfacial conductances at the two interfaces are assumed for simplicity. Following the similar procedure as presented in the previous section for the derivation of Eq. (9), the expressions of $\mathbf{Q}_{1(2)}$ can be solved with the resulting torques defined by Eq. (23). The detailed derivation steps can be found in the Appendix.

When only ANE in the F1 contributes (i.e., $N_{\mathrm{SNE}} = 0$), the spin torque is derived as

$$\boldsymbol{T}_{\mathrm{ANE}} = A_{\mathrm{ANE}} m_{y1} \boldsymbol{m}_2 \times (\boldsymbol{m}_1 \times \boldsymbol{m}_2), \tag{24}$$

where $(A_{\mathrm{ANE}} m_{y1})$ is proportional to $\mu^0_{\mathrm{ANE}}$ with $\mu^0_{\mathrm{ANE}} = \frac{e}{g_{\mathrm{F1}}} \tanh(\frac{t_{\mathrm{F1}}}{2\lambda_{\mathrm{F1}}}) j_{\mathrm{ANE}}$. $A_{\mathrm{ANE}}$ gives the compact form of the spin torque magnitude due to ANE, which is a function of material parameters, e.g., $N_{\mathrm{ANE}}$, $G_\uparrow$, $G_\downarrow$, $G_r$, etc. Note that $m_{y1}$ appears in Eq. (24) since it is included in the expression of $j_{\mathrm{ANE}}$ [Eq. (5)], indicating that a nonzero $m_{y1}$ in F1 is required to exert a spin torque on F2 within the mechanism of ANE. On the other hand, when only SNE in the N contributes (i.e., $N_{\mathrm{ANE}} = 0$), the spin torque has the form of

$$\begin{aligned}\boldsymbol{T}_{\mathrm{SNE}} = {} & B_{\mathrm{SNE},1} \boldsymbol{m}_2 \times (\hat{\boldsymbol{y}} \times \boldsymbol{m}_2) + B_{\mathrm{SNE},2} m_{y1} \boldsymbol{m}_2 \times (\boldsymbol{m}_1 \times \boldsymbol{m}_2) \\ & + B_{\mathrm{SNE},3} m_{y2} (\boldsymbol{m}_1 \cdot \boldsymbol{m}_2) \boldsymbol{m}_2 \times (\boldsymbol{m}_1 \times \boldsymbol{m}_2),\end{aligned} \tag{25}$$

where $B_{\mathrm{SNE},1-3}$ is proportional to $\mu^0_{\mathrm{SNE}}$ with $\mu^0_{\mathrm{SNE}} = \frac{e}{g_{\mathrm{N1}}} \tanh(\frac{t_{\mathrm{N1}}}{2\lambda_{\mathrm{N1}}}) j_{\mathrm{SNE}}$. $B_{\mathrm{SNE},1-3}$ give the compact form of the spin torque magnitude with respect to three different angular dependencies due to SNE. The first term of Eq. (25) with respect to $B_{\mathrm{SNE},1}$ has the same form as the conventional (dampinglike) spin Hall torque [$\sim \boldsymbol{m}_2 \times (\hat{\boldsymbol{y}} \times \boldsymbol{m}_2)$]. Meanwhile, the magnetization of F1 (i.e., $\boldsymbol{m}_1$) also affects the SNE-generated torque exerting on F2, as represented by the remaining two terms in Eq. (25). When both ANE and SNE exist, the total spin torque is given simply by the sum of both contributions, i.e.,

$$\boldsymbol{T} = \boldsymbol{T}_{\mathrm{ANE}} + \boldsymbol{T}_{\mathrm{SNE}}. \tag{26}$$

Next, we theoretically investigate how the above spin torques from the SNE and ANE influence the FMR in the free F2 layer and thus provide a means of characterizing the two thermoelectric effects. Here we consider a classical microwave-driven FMR to which the spin torque enters as a quantity that influences the precessional motion which in turn can be detected by a change in the FMR linewidth. The Laudau-Lifshitz Gilbert (LLG) equation of the free F2 magnetization $\boldsymbol{m}_2$ can be expressed as

$$\frac{d\boldsymbol{m}_2}{dt} = -\gamma \mu_0 \boldsymbol{m}_2 \times \mathbf{H}_{\mathrm{eff}} + \alpha \boldsymbol{m}_2 \times \frac{d\boldsymbol{m}_2}{dt} + \frac{\hbar}{2e} \frac{\gamma}{M_s t_{\mathrm{F2}}} \boldsymbol{T}, \tag{27}$$

where $\mathbf{H}_{\mathrm{eff}} = \mathbf{H}_{\mathrm{ex}} + \mathbf{H}_{\mathrm{D}} + \mathbf{H}_{\mathrm{uni}} + \mathbf{h}$ with the static external magnetic field $\mathbf{H}_{\mathrm{ex}}$, demagnetization field $\mathbf{H}_{\mathrm{D}}$, uniaxial in-plane magnetocrystalline anisotropy $\mathbf{H}_{\mathrm{uni}}$, and a small uniform excitation field $\mathbf{h}$ pointing perpendicular to $\mathbf{H}_{\mathrm{ex}}$. $\gamma$, $\mu_0$, $\alpha$, $M_s$, and $t_{\mathrm{F2}}$ are the gyromagnetic ratio, vacuum permeability, Gilbert damping constant of the isolated layer, saturation magnetization, and thickness of the F2 layer, respectively. Here the spin torque $\boldsymbol{T}$ is multiplied with the prefactor $\frac{\hbar}{2e} \frac{\gamma}{M_s t_{\mathrm{F2}}}$. Therefore, the torque acts over the entire thickness of the free F2 layer ($t_{\mathrm{F2}}$) and represents a bulk effect arising from the interfacial spin current density. As shown in Fig. 4(b), the static external magnetic field $\mathbf{H}_{\mathrm{ex}}$ is applied at a polar angle $\varphi_{\mathrm{H}}$ in the $x$-$y$ plane. We consider the magnetization dynamics in the transformed $XYZ$-coordinate system [Fig. 4(b)], in which the magnetization is stabilized along the $Y$ axis with a sufficiently large external magnetic field, i.e., $\mathbf{H}_{\mathrm{ex}} = H_{\mathrm{ex}} \hat{\boldsymbol{Y}}$. As $\mathbf{h} \ll \mathbf{H}_{\mathrm{ex}}$, we expect the excitation field to sustain a small-angle precession about the $Y$ axis. Consequently, the unit magnetization $\boldsymbol{m}_2$ can be decomposed into static and dynamic components as $\boldsymbol{m}_2 = m_{2X} \hat{\boldsymbol{X}} + \hat{\boldsymbol{Y}} + m_{2Z} \hat{\boldsymbol{Z}}$, where $m_{2X}$ and $m_{2Z}$ are the oscillating high frequency components in the $XYZ$ coordinate. Equivalently, the total magnetization $\boldsymbol{M}_2 = M_s \boldsymbol{m}_2$ is given by $\boldsymbol{M}_2 = M_{2X} \hat{\boldsymbol{X}} + M_s \hat{\boldsymbol{Y}} + M_{2Z} \hat{\boldsymbol{Z}}$ with $M_{2X(Z)} = M_s m_{2X(Z)}$. With the excitation field being $\mathbf{h} = h e^{i\omega t} \hat{\boldsymbol{X}}$, the resulting small-angle precession around the equilibrium direction about $\hat{\boldsymbol{Y}}$ is described by $m_{2X}(t) = \delta m_{2X} e^{i\omega t}$ and $m_{2Z}(t) = \delta m_{2Z} e^{i\omega t}$. In this section, we consider that both $\boldsymbol{m}_1$ and $\boldsymbol{m}_2$ of the two F layers are oriented in-plane with polar angles $\varphi_1$ and $\varphi_2$, respectively, as illustrated in Fig. 4(b). Linearization of the LLG equation [i.e., Eq. (28)] with respect to $\boldsymbol{m}_2$ leads to the equation

$$\omega_M \begin{pmatrix} h \\ 0 \end{pmatrix} = \begin{pmatrix} i\omega\alpha + \omega_{\mathrm{H}} & i\omega + \omega_N \\ -i\omega - \omega_N & i\omega\alpha + \omega_{\mathrm{H}} + \omega_{\mathrm{D}} \end{pmatrix} \begin{pmatrix} M_{2X} \\ M_{2Z} \end{pmatrix}. \tag{28}$$

$\omega_M$, $\omega_{\mathrm{H}}$, and $\omega_{\mathrm{D}}$ are convenient abbreviations with $\omega_M = \gamma \mu_0 M_s$, $\omega_{\mathrm{H}} = \gamma \mu_0 (H_{\mathrm{ex}} + H_{\mathrm{uni}})$, and $\omega_{\mathrm{D}} = \gamma \mu_0 M_{\mathrm{eff}}$, respectively, where $\mathbf{H}_{\mathrm{uni}} = H_{\mathrm{uni}} \hat{\boldsymbol{Y}}$ and $\mathbf{H}_{\mathrm{D}} = -M_{\mathrm{eff}} m_{2Z} \hat{\boldsymbol{Z}}$ are considered. Note that $\omega_N$ represents the frequency originating from SNE and ANE with

$$\omega_N = \frac{\hbar}{2e} \frac{\gamma}{M_s t_{\mathrm{F2}}} (A_{\mathrm{ANE}} + B_{\mathrm{SNE},1} + B_{\mathrm{SNE},2} + B_{\mathrm{SNE},3}) \sin \varphi_{\mathrm{H}}, \tag{29}$$

where $\varphi_1 = \varphi_2 = \varphi_{\mathrm{H}}$ is used for simplicity. Note that $A_{\mathrm{ANE}}$ and $B_{\mathrm{SNE},1-3}$ are proportional to $j_{\mathrm{ANE}} = m_y (p - \beta_{\mathrm{F}}) \sigma_{\mathrm{F}} N_{\mathrm{ANE}} \partial_x T$ and $j_{\mathrm{SNE}} = \sigma_{\mathrm{N}} N_{\mathrm{SNE}} \partial_x T$, respectively. Except for the $\partial_x T$ dependence, other parameters in the expression of $\omega_N$ are material dependent and can be treated as constants. Compared with the conventional frequency terms induced by the external magnetic field, anisotropy field, and demagnetization field (i.e., $\omega_{\mathrm{H}}$ and $\omega_{\mathrm{D}}$), we focus on the modulation of the FMR by the SNE and ANE which is represented by $\omega_N$. Rearranging Eq. (28), the susceptibility tensor $\bar{\bar{\chi}}$ can be obtained as

$$\begin{pmatrix} M_{2X} \\ M_{2Z} \end{pmatrix} = \boldsymbol{M}_2 = \bar{\bar{\chi}} \mathbf{h} = \begin{pmatrix} \chi_{XX} & \chi_{XZ} \\ \chi_{ZX} & \chi_{ZZ} \end{pmatrix} \begin{pmatrix} h \\ 0 \end{pmatrix}. \tag{30}$$

Therefore, the real and imaginary parts of the susceptibility tensor component $\chi_{XX} = \chi'_{XX} - i\chi''_{XX}$ are given by

$$\chi'_{XX} = \frac{\omega_M\left[(\omega_H + \omega_D)\left(\omega_{res}^2 - \omega^2\right) + 2\alpha\omega_N\omega^2\right]}{\left(\omega_{res}^2 - \omega^2\right)^2 + \omega^2[\alpha(2\omega_H + \omega_D) + 2\omega_N]^2}, \tag{31}$$

$$\chi''_{XX} = \frac{\omega_M\omega\{\alpha[\omega^2 - \omega_N^2 + (2\omega_H + \omega_D)^2] + 2\omega_N(\omega_H + \omega_D)\}}{\left(\omega_{res}^2 - \omega^2\right)^2 + \omega^2[\alpha(2\omega_H + \omega_D) + 2\omega_N]^2}, \tag{32}$$

where the resonance frequency $\omega_{res}$ is introduced as

$$\omega_{res}^2 = \omega_H(\omega_H + \omega_D) + \omega_N^2. \tag{33}$$

It is supposed that $\alpha \ll 1$, $1 + \alpha^2 \approx 1$ is utilized in deriving Eqs. (31) and (32). The real part $\chi'_{XX}$ represents the component of $m_{2X}$ that is in phase with the excitation field **h**, and the imaginary part $\chi''_{XX}$ denotes its component which is delayed from **h** with a phase angle of $\pi/2$. When there is neither SNE nor ANE contributions (i.e., $\omega_N = 0$), $\chi'_{XX}$ becomes zero at the resonance condition (i.e., $\omega = \omega_{res}$). The frequency linewidth is also obtained from Eqs. (31) and (32) as

$$\Delta\omega = \tfrac{1}{2}[\alpha(2\omega_H + \omega_D) + 2\omega_N]. \tag{34}$$

Consequently, the field-swept linewidth $\Delta H$ can be calculated as

$$\Delta H = \frac{1}{\mu_0\gamma}\left(\frac{d\omega_{res}}{d\omega_H}\right)^{-1}\Delta\omega = \frac{\omega_{res}}{\mu_0\gamma}\left(\alpha + \frac{2\omega_N}{\omega_D + 2\omega_H}\right). \tag{35}$$

Based on above derivation, it can be seen that the FMR resonance amplitude and linewidth are modulated by SNE and ANE (i.e., $\omega_N$).

For the numerical calculation, we consider a NiFe(F1)/Pt(N)/CoFeB(F2) structure with the same material parameters as introduced previously. The additional parameters for the free F2 made of CoFeB are [6,7,39] $t_{F2} = 1.7$ nm, $\rho_{F2} = 300\ \Omega$ nm, $\lambda_{F2} = 4.5$ nm, $\beta_{F2} = 0.56$, $\mu_0 M_s = 1\ \mathrm{T} \approx \mu_0 M_{eff}$, and $\alpha = 0.01$. $H_{uni}$ is treated as negligible compared with the applied $H_{ex}$ [39]. The frequency of the microwave field $\omega$ is 9.53 GHz [40]. Here we perform the FMR measurement by fixing $\omega$ and sweeping $H_{ex}$, i.e., $\chi'_{XX}$ and $\chi''_{XX}$ are plotted as a function of the static external field $H_{ex}$ in Figs. 5(a) and 5(b), respectively, where an antisymmetric and a symmetric spectrum are observed. With the effects of both SNE and ANE, the magnitude of the susceptibility is enhanced additively. Note that the magnitude will be decreased when $\nabla T$ is applied in the opposite direction. In Figs. 5(a) and 5(b), a large temperature gradient of $\partial_x T = 1$ K/nm is utilized. Next, we plot $\chi''_{XX}$ and $\Delta H$ as a function of $\partial_x T$ at the resonance condition in Figs. 5(c) and 5(d), respectively, in which the additive effects of SNE and ANE can also be observed and the effects of them become significant only at large temperature gradient exceeding $\partial_x T \sim 0.1$ K/nm. It is only at such large thermal gradients that $\omega_N$ gives an observable effect on the resonance amplitude [via Eqs. (31) and (32)] and linewidth [via Eq. (35)], e.g., with the field linewidth $\Delta H$ change of the order of 10 Oe by SNE and ANE. Further, a larger $\partial_x T$ on the scale of 1 K/nm is required to achieve a comparable $\omega_N$ with $\omega_H$, i.e., $\omega_N \sim 0.1$ GHz with $\omega_H \sim 0.5$ GHz at resonance. Note that the FMR spectrum is independent of the length and width of the sample for a fixed $\nabla T$, unlike the TSMR voltage measurement as described in the previous section, and is therefore limited by the small value of $N_{ANE(SNE)}$ of at most several $\mu$V/K. As a result, most available experimental works investigating the thermal Hall effects are based on the TSMR (i.e., voltage) measurement [8,10,13,15]. Nevertheless, our derivation yields the analytical expression of the FMR outputs under the SNE and ANE, and predicts that it can provide an alternative albeit a less sensitive route to the detection of SNE and ANE. On the other hand, although conventional Joule heater might have limitations for generating a large temperature gradient for observable Nernst effects based on the FMR output, it can still be realized experimentally via other means, e.g., by laser heating [41].

As indicated before, here we consider a classical microwave-driven FMR with a microwave excitation field **h**. On the other hand, FMR excited by an rf current has also been extensively investigated recently [4,42,43]. This current-driven FMR is not adopted in this work since the excitation rf current itself may induce additional spin torques originating from SHE and AHE at the same time. However, in the specific configuration where the magnetizations in F1 and F2 are parallel, the rf spin-transfer torques due to the oscillating current would not affect the FMR spectrum [44,45].

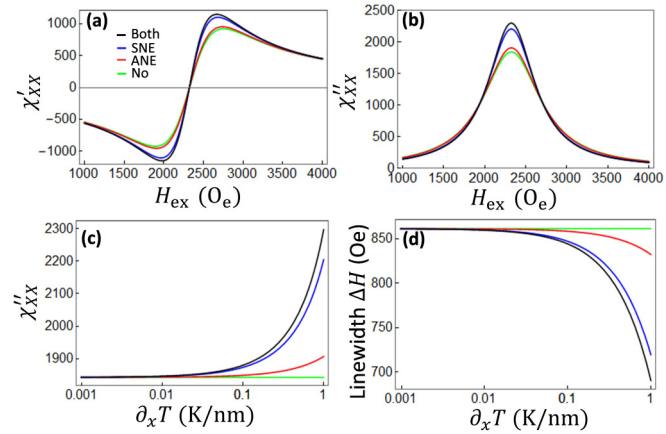


FIG. 5. FMR analysis of the spin torques. (a) $\chi'_{XX}$ (i.e., the real part of the susceptibility $\chi_{XX}$) as a function of the applied external field $H_{ex}$. (b) $\chi''_{XX}$ (i.e., the imaginary part of the susceptibility $\chi_{XX}$) as a function of $H_{ex}$. (c) $\chi''_{XX}$ as a function of the applied in-plane temperature gradient $\partial_x T$ at the resonance condition. (d) The field-swept linewidth $\Delta H$ as a function of $\partial_x T$ at the resonance condition. The blue, red, black, and green lines represent contributions from only SNE, only ANE, both and neither of them, respectively. In (a) and (b), $\partial_x T = 1$ K/nm is utilized.

Therefore, the expressions of the resonance frequency and linewidth derived above [i.e., Eq. (33)–(35)] are also valid for the rf current-driven FMR since we have adopted $\varphi_1 = \varphi_2 = \varphi_H$ (parallel magnetization configuration) in our derivation, for simplicity. Under this condition, the excitation field **h** used in this work can be replaced by the rf current-induced Oersted field instead. Therefore, the rf current-driven FMR would also require a large thermal gradient to generate sufficient spin torque for an observable signal, similar to that of the classical microwave-driven FMR discussed in this work.

## III. CONCLUSION

In this work, we present a phenomenological spin transport theory based on drift-diffusion equations to treat SNE and ANE simultaneously in F/N heterostructures, and analyze their signature outputs. In a F/N bilayer with an in-plane temperature gradient, the analytical expressions of the TSMR voltage originating from SNE in N and ANE in F are derived, in which SNE and ANE give additive (opposing) contributions for the transverse (longitudinal) voltages when considering the Nernst coefficients of SNE and ANE are of the same sign. The anisotropic contributions of SNE and ANE to the TSMR voltage provide a possible means of separating out the individual contributions of SNE and ANE, as well as information on the spin-dependent polarization parameters in F. On the other hand, based on a F1/N/F2 trilayer, we investigate the spin torques acting on the additional F2 resulting from SNE in N and ANE in F1 by analyzing the FMR outputs. The FMR spectrum and linewidth are calculated analytically and numerically. For the magnetization configuration considered, the SNE and ANE contribute additively to the resonance magnitude and linewidth. Although the available $N_{\mathrm{ANE(SNE)}}$ is limited to the order of several $\mu$V/K, a comparison of the two signature outputs shows that unlike the FMR outputs, the TSMR voltage arising from SNE and ANE can be enhanced by using the sample with larger dimensions, and therefore provides a more sensitive measurement of the thermally induced spin transport effects.

## ACKNOWLEDGMENTS

This work was supported by the Singapore National Research Foundation (NRF), Prime Minister's Office, under its Competitive Research Programme (NRF CRP12-2013-01, NUS Grant No. R-263-000-B30-281), Ministry of Education (MOE) Tier-II Grant No. MOE2018-T2-2-117 (NUS Grant No. R-398-000-092-112), MOE Tier-I FRC grant (NUS Grant No. R-263-000-D66-114), and other MOE grants (NUS Grants No. C-261-000-207-532 and No. C-261-000-777-532).

## APPENDIX: DERIVATION OF THE SPIN TORQUE

Following a similar procedure as presented in Sec. II B for a F/N bilayer, we now consider the F1/N/F2 trilayer (Fig. 4). Similarly, $\mathbf{Q}_{1(2)}$ is introduced as the interfacial spin current density at the F1(F2)/N interface, which is defined as being injected from F1(F2) to N.

In the N layer, we apply two boundary conditions on the N side of the interfaces, i.e., $\boldsymbol{j}_{sz,\mathrm{N}}(L_1) = \mathbf{Q}_1$ and $\boldsymbol{j}_{sz,\mathrm{N}}(L_2) = -\mathbf{Q}_2$; the expression of the spin accumulation in the N can be solved from the aforementioned drift-diffusion equation in terms of $\mathbf{Q}_1$ and $\mathbf{Q}_2$ as

$$\boldsymbol{\mu}_{s,\mathrm{N}} = \frac{e}{g_{\mathrm{N}}}\left[\frac{\cosh\left(\frac{t_{\mathrm{F1}}+t_{\mathrm{N}}-z}{\lambda_{\mathrm{N}}}\right)}{\sinh\left(\frac{t_{\mathrm{N}}}{\lambda_{\mathrm{N}}}\right)}\mathbf{Q}_1 + \frac{\cosh\left(\frac{t_{\mathrm{F1}}-z}{\lambda_{\mathrm{N}}}\right)}{\sinh\left(\frac{t_{\mathrm{N}}}{\lambda_{\mathrm{N}}}\right)}\mathbf{Q}_2 + j_{\mathrm{SNE}}\mathrm{sech}\left(\frac{t_{\mathrm{N}}}{2\lambda_{\mathrm{N}}}\right)\sinh\left(\frac{2t_{\mathrm{F1}}+t_{\mathrm{N}}-2z}{2\lambda_{\mathrm{N}}}\right)\hat{\boldsymbol{y}}\right]. \tag{A1}$$

Accordingly, the spin accumulations at the boundaries (on the N side) are explicitly given by

$$\boldsymbol{\mu}_{s,\mathrm{N}}(L_1) = \frac{e}{g_{\mathrm{N}}}\left[\coth\left(\frac{t_{\mathrm{N}}}{\lambda_{\mathrm{N}}}\right)\mathbf{Q}_1 + \mathrm{csch}\left(\frac{t_{\mathrm{N}}}{\lambda_{\mathrm{N}}}\right)\mathbf{Q}_2 - j_{\mathrm{SNE}}\tanh\left(\frac{t_{\mathrm{N}}}{2\lambda_{\mathrm{N}}}\right)\hat{\boldsymbol{y}}\right] \tag{A2}$$

and

$$\boldsymbol{\mu}_{s,\mathrm{N}}(L_2) = \frac{e}{g_{\mathrm{N}}}\left[\mathrm{csch}\left(\frac{t_{\mathrm{N}}}{\lambda_{\mathrm{N}}}\right)\mathbf{Q}_1 + \coth\left(\frac{t_{\mathrm{N}}}{\lambda_{\mathrm{N}}}\right)\mathbf{Q}_2 + j_{\mathrm{SNE}}\tanh\left(\frac{t_{\mathrm{N}}}{2\lambda_{\mathrm{N}}}\right)\hat{\boldsymbol{y}}\right]. \tag{A3}$$

In the F1 with ANE, we apply $j_{sz,\mathrm{F1}}(0) = 0$ and $j_{sz,\mathrm{F1}}(L_1) = \boldsymbol{m}_1 \cdot \mathbf{Q}_1$, with which the spin accumulation can be solved from the drift-diffusion equation in terms of $\mathbf{Q}_1$ as

$$\mu_{s,\mathrm{F1}} = -\frac{e}{g_{\mathrm{F1}}}\frac{1}{\sinh\left(\frac{t_{\mathrm{F1}}}{\lambda_{\mathrm{F1}}}\right)}\left[2j_{\mathrm{ANE}}\sinh\left(\frac{t_{\mathrm{F1}}}{2\lambda_{\mathrm{F1}}}\right)\sinh\left(\frac{t_{\mathrm{F1}}-2z}{2\lambda_{\mathrm{F1}}}\right) + \cosh\left(\frac{z}{\lambda_{\mathrm{F1}}}\right)\boldsymbol{m}_1 \cdot \mathbf{Q}_1\right]. \tag{A4}$$

Accordingly, the spin accumulation at $z = L_1$ (on the F1 side) is given by

$$\mu_{s,\mathrm{F1}}(L_1) = -\frac{e}{g_{\mathrm{F1}}}\left[-j_{\mathrm{ANE}}\tanh\left(\frac{t_{\mathrm{F1}}}{2\lambda_{\mathrm{F1}}}\right) + \coth\left(\frac{t_{\mathrm{F1}}}{\lambda_{\mathrm{F1}}}\right)\boldsymbol{m}_1 \cdot \mathbf{Q}_1\right]. \tag{A5}$$

Similarly, in the F2 without ANE (i.e., $N_{\mathrm{ANE}} = 0$), by applying $j_{sz,\mathrm{F2}}(L_2) = -\boldsymbol{m}_2 \cdot \mathbf{Q}_2$ and $j_{sz,\mathrm{F2}}(L_3) = 0$, the spin accumulation can be obtained as

$$\mu_{s,\mathrm{F2}} = -\frac{e}{g_{\mathrm{F2}}}\frac{1}{\sinh\left(\frac{t_{\mathrm{F2}}}{\lambda_{\mathrm{F2}}}\right)}\cosh\left(\frac{t_{\mathrm{F1}}+t_{\mathrm{N}}+t_{\mathrm{F2}}-z}{\lambda_{\mathrm{F2}}}\right)\boldsymbol{m}_2 \cdot \mathbf{Q}_2. \tag{A6}$$

The spin accumulation at $z = L_2$ (on the F2 side) is given by

$$\mu_{s,\mathrm{F2}}(L_2) = -\frac{e}{g_{\mathrm{F2}}}\coth\left(\frac{t_{\mathrm{F2}}}{\lambda_{\mathrm{F2}}}\right)\boldsymbol{m}_2\cdot\mathbf{Q}_2. \tag{A7}$$

With the same form as Eq. (8), we have the boundary condition at the F1/N interface (i.e., $z = L_1$) as

$$e\mathbf{Q}_1 = G_0[\mu_{s,\mathrm{F1}}(L_1) - \boldsymbol{m}_1\cdot\boldsymbol{\mu}_{s,\mathrm{N}}(L_1)]\boldsymbol{m}_1 + 2G_r\boldsymbol{m}_1\times[\boldsymbol{m}_1\times\boldsymbol{\mu}_{s,\mathrm{N}}(L_1)] + 2G_i[\boldsymbol{m}_1\times\boldsymbol{\mu}_{s,\mathrm{N}}(L_1)], \tag{A8}$$

Applying $G_i = 0$ and multiplying $1/e$, Eq. (A8) becomes

$$\mathbf{Q}_1 = G_0\left[\frac{\mu_{s,\mathrm{F1}}(L_1)}{e} - \boldsymbol{m}_1\cdot\frac{\boldsymbol{\mu}_{s,\mathrm{N}}(L_1)}{e}\right]\boldsymbol{m}_1 + 2G_r\boldsymbol{m}_1\times\left[\boldsymbol{m}_1\times\frac{\boldsymbol{\mu}_{s,\mathrm{N}}(L_1)}{e}\right]. \tag{A9}$$

For notational simplification, we rewrite Eqs. (A5) and (A2), respectively, as

$$\frac{\mu_{s,\mathrm{F1}}(L_1)}{e} = \frac{\mu^0_{\mathrm{ANE}}}{e} - \frac{1}{G_{\mathrm{F1}}}(\boldsymbol{m}_1\cdot\mathbf{Q}_1), \tag{A10}$$

and

$$\frac{\boldsymbol{\mu}_{s,\mathrm{N}}(L_1)}{e} = \frac{1}{G_{11}}\mathbf{Q}_1 + \frac{1}{G_{12}}\mathrm{Q}_2 - \frac{\mu^0_{\mathrm{SNE}}}{e}\hat{\boldsymbol{y}}, \tag{A11}$$

where the effective conductances are given by $G_{\mathrm{F1}} = g_{\mathrm{F1}}\tanh(\frac{t_{\mathrm{F1}}}{\lambda_{\mathrm{F1}}})$, $G_{11} = g_{\mathrm{N}}\tanh(\frac{t_{\mathrm{N}}}{\lambda_{\mathrm{N}}})$, and $G_{12} = g_{\mathrm{N}}\sinh(\frac{t_{\mathrm{N}}}{\lambda_{\mathrm{N}}})$. Substituting Eqs. (A10) and (A11) into Eq. (A9), we get

$$\mathbf{Q}_1 = D_1\boldsymbol{m}_1 + D_2(\boldsymbol{m}_1\cdot\mathbf{Q}_1)\boldsymbol{m}_1 + D_3(\boldsymbol{m}_1\cdot\mathbf{Q}_2)\boldsymbol{m}_1 + D_4\boldsymbol{m}_1\times(\boldsymbol{m}_1\times\mathbf{Q}_2) + D_5\boldsymbol{m}_1\times(\boldsymbol{m}_1\times\mathbf{Q}_1) + D_6\boldsymbol{m}_1\times(\boldsymbol{m}_1\times\hat{\boldsymbol{y}}), \tag{A12}$$

where $D_1 = (\frac{\mu^0_{\mathrm{ANE}}}{e} + \frac{\mu^0_{\mathrm{SNE}}}{e}m_{y1})G_0$, $D_2 = -(\frac{1}{G_{\mathrm{F1}}} + \frac{1}{G_{11}})G_0$, $D_3 = -\frac{G_0}{G_{12}}$, $D_4 = \frac{2G_r}{G_{12}}$, $D_5 = \frac{2G_r}{G_{11}}$, and $D_6 = -\frac{2\mu^0_{\mathrm{SNE}}}{e}G_r$. Based on Eq. (A12), we obtain three more equations with respect to $\boldsymbol{m}_1$, i.e.,

$$\boldsymbol{m}_1\cdot\mathbf{Q}_1 = D_1 + D_2(\boldsymbol{m}_1\cdot\mathbf{Q}_1) + D_3(\boldsymbol{m}_1\cdot\mathbf{Q}_2), \tag{A13}$$

$$\boldsymbol{m}_1\times\mathbf{Q}_1 = -D_4(\boldsymbol{m}_1\times\mathbf{Q}_2) - D_5(\boldsymbol{m}_1\times\mathbf{Q}_1) - D_6(\boldsymbol{m}_1\times\hat{\boldsymbol{y}}), \tag{A14}$$

and

$$\boldsymbol{m}_1\times(\boldsymbol{m}_1\times\mathbf{Q}_1) = -D_4\boldsymbol{m}_1\times(\boldsymbol{m}_1\times\mathbf{Q}_2) - D_5\boldsymbol{m}_1\times(\boldsymbol{m}_1\times\mathbf{Q}_1) - D_6\boldsymbol{m}_1\times(\boldsymbol{m}_1\times\hat{\boldsymbol{y}}). \tag{A15}$$

Applying the same algebraic procedures with respect to $\boldsymbol{m}_2$ to Eq. (A12), giving

$$\begin{aligned}\boldsymbol{m}_2\cdot\mathbf{Q}_1 = {} & D_1(\boldsymbol{m}_1\cdot\boldsymbol{m}_2) + D_2(\boldsymbol{m}_1\cdot\boldsymbol{Q}_1)(\boldsymbol{m}_1\cdot\boldsymbol{m}_2) + D_3(\boldsymbol{m}_1\cdot\boldsymbol{Q}_2)(\boldsymbol{m}_1\cdot\boldsymbol{m}_2) + D_4[(\boldsymbol{m}_1\cdot\boldsymbol{Q}_2)(\boldsymbol{m}_1\cdot\boldsymbol{m}_2)\\ & - (\boldsymbol{m}_2\cdot\boldsymbol{Q}_2)] + D_5[(\boldsymbol{m}_1\cdot\boldsymbol{Q}_1)(\boldsymbol{m}_1\cdot\boldsymbol{m}_2) - (\boldsymbol{m}_2\cdot\boldsymbol{Q}_1)] + D_6[\boldsymbol{m}_{y1}\cdot(\boldsymbol{m}_1\cdot\boldsymbol{m}_2) - \boldsymbol{m}_{y2}],\end{aligned} \tag{A16}$$

$$\begin{aligned}\boldsymbol{m}_2\times\mathbf{Q}_1 = {} & D_1(\boldsymbol{m}_2\times\boldsymbol{m}_1) + D_2(\boldsymbol{m}_1\cdot\mathbf{Q}_1)(\boldsymbol{m}_2\times\boldsymbol{m}_1) + D_3(\boldsymbol{m}_1\cdot\mathbf{Q}_2)(\boldsymbol{m}_2\times\boldsymbol{m}_1) + D_4[(\boldsymbol{m}_1\cdot\mathbf{Q}_2)(\boldsymbol{m}_2\cdot\boldsymbol{m}_1)\\ & - (\boldsymbol{m}_2\times\mathbf{Q}_2)] + D_5[(\boldsymbol{m}_1\cdot\mathbf{Q}_1)(\boldsymbol{m}_2\times\boldsymbol{m}_1) - (\boldsymbol{m}_2\times\mathbf{Q}_1)] + D_6[m_{y1}(\boldsymbol{m}_2\times\boldsymbol{m}_1) - \boldsymbol{m}_2\times\hat{\boldsymbol{y}}],\end{aligned} \tag{A17}$$

$$\begin{aligned}\boldsymbol{m}_2\times(\boldsymbol{m}_2\times\mathbf{Q}_1) = {} & D_1\boldsymbol{m}_2\times(\boldsymbol{m}_2\times\boldsymbol{m}_1) + D_2(\boldsymbol{m}_1\cdot\mathbf{Q}_1)\boldsymbol{m}_2\times(\boldsymbol{m}_2\times\boldsymbol{m}_1) + D_3(\boldsymbol{m}_1\cdot\mathbf{Q}_2)\boldsymbol{m}_2\\ & \times(\boldsymbol{m}_2\cdot\boldsymbol{m}_1) + D_4[(\boldsymbol{m}_1\cdot\mathbf{Q}_2)\boldsymbol{m}_2\times(\boldsymbol{m}_2\times\boldsymbol{m}_1) - \boldsymbol{m}_2\times(\boldsymbol{m}_2\times\mathbf{Q}_2)] + D_5[(\boldsymbol{m}_1\cdot\mathbf{Q}_1)\boldsymbol{m}_2\times(\boldsymbol{m}_2\times\boldsymbol{m}_1) - \boldsymbol{m}_2\\ & \times(\boldsymbol{m}_2\times\mathbf{Q}_1)] + D_6[m_{y1}\boldsymbol{m}_2\times(\boldsymbol{m}_2\times\boldsymbol{m}_1) - \boldsymbol{m}_2\times(\boldsymbol{m}_2\times\hat{\boldsymbol{y}})].\end{aligned} \tag{A18}$$

Therefore, we get six equations from Eq. (A9), i.e., Eqs. (A13)–(A18).

At the F2/N interface (i.e., $z = L_2$), similar to Eq. (A9), we have

$$\mathbf{Q}_2 = G_0\left[\frac{\mu_{s,\mathrm{F2}}(L_2)}{e} - \boldsymbol{m}_2\cdot\frac{\boldsymbol{\mu}_{s,\mathrm{N}}(L_2)}{e}\right]\boldsymbol{m}_2 + 2G_r\boldsymbol{m}_2\times\left[\boldsymbol{m}_2\times\frac{\boldsymbol{\mu}_{s,\mathrm{N}}(L_2)}{e}\right]. \tag{A19}$$

Equations (A6) and (A3) are rewritten, respectively, as

$$\frac{\mu_{s,\mathrm{F2}}(L_2)}{e} = -\frac{1}{G_{\mathrm{F2}}}(\boldsymbol{m}_2\cdot\mathbf{Q}_2), \tag{A20}$$

and

$$\frac{\boldsymbol{\mu}_{s,\mathrm{N}}(L_2)}{e} = \frac{1}{G_{12}}\mathbf{Q}_1 + \frac{1}{G_{11}}\mathbf{Q}_2 + \frac{\mu^0_{\mathrm{SNE}}}{e}\hat{\boldsymbol{y}}, \tag{A21}$$

where $G_{F2} = g_{F2}\tanh(\frac{t_{F2}}{\lambda_{F2}})$. Substituting Eqs. (A20) and (A21) into Eq. (A19) with the same algebraic transformations, another six equations of $\boldsymbol{m}_1 \cdot \mathbf{Q}_2$, $\boldsymbol{m}_1 \times \mathbf{Q}_2$, $\boldsymbol{m}_1 \times (\boldsymbol{m}_1 \times \mathbf{Q}_2)$, $\boldsymbol{m}_2 \cdot \mathbf{Q}_2$, $\boldsymbol{m}_2 \times \mathbf{Q}_2$, and $\boldsymbol{m}_2 \times (\boldsymbol{m}_2 \times \mathbf{Q}_2)$ can be obtained accordingly.

Then, we have 12 linear equations with 12 unknowns in terms of $\mathbf{Q}_1$ and $\mathbf{Q}_2$. The 12 unknowns are $\boldsymbol{m}_1 \cdot \mathbf{Q}_1$, $\boldsymbol{m}_1 \cdot \mathbf{Q}_2$, $\boldsymbol{m}_2 \cdot \mathbf{Q}_1$, $\boldsymbol{m}_2 \cdot \mathbf{Q}_2$, $\boldsymbol{m}_1 \times \mathbf{Q}_1$, $\boldsymbol{m}_1 \times \mathbf{Q}_2$, $\boldsymbol{m}_2 \times \mathbf{Q}_1$, $\boldsymbol{m}_2 \times \mathbf{Q}_2$, $\boldsymbol{m}_1 \times (\boldsymbol{m}_1 \times \mathbf{Q}_1)$, $\boldsymbol{m}_1 \times (\boldsymbol{m}_1 \times \mathbf{Q}_2)$, $\boldsymbol{m}_2 \times (\boldsymbol{m}_2 \times \mathbf{Q}_1)$, and $\boldsymbol{m}_2 \times (\boldsymbol{m}_2 \times \mathbf{Q}_2)$, in which $\boldsymbol{m}_2 \times (\boldsymbol{m}_2 \times \mathbf{Q}_2)$ gives the spin torque defined by Eq. (23). Subsequently, the expression of the spin torque solution is solved with the unknown $\boldsymbol{m}_2 \times (\boldsymbol{m}_2 \times \mathbf{Q}_2)$. By setting $N_{SNE} = 0$, we would be able to obtain the expression for the coefficient $A_{ANE}$ in Eq. (24) which represents the ANE contribution to the spin torque. Similarly, by setting $N_{ANE} = 0$, we would obtain the expressions for the three coefficients $B_{SNE,1-3}$ in Eq. (25), which represent the SNE contribution to the spin torque.


[1] J. E. Hirsch, Phys. Rev. Lett. **83**, 1834 (1999).
[2] J. Sinova, D. Culcer, Q. Niu, N. A. Sinitsyn, T. Jungwirth, and A. H. MacDonald, Phys. Rev. Lett. **92**, 126603 (2004).
[3] L. Liu, C.-F. Pai, Y. Li, H. Tseng, D. Ralph, and R. Buhrman, Science **336**, 555 (2012).
[4] L. Liu, T. Moriyama, D. C. Ralph, and R. A. Buhrman, Phys. Rev. Lett. **106**, 036601 (2011).
[5] N. Nagaosa, J. Sinova, S. Onoda, A. H. MacDonald, and N. P. Ong, Rev. Mod. Phys. **82**, 1539 (2010).
[6] T. Taniguchi, J. Grollier, and M. D. Stiles, Phys. Rev. Appl. **3**, 044001 (2015).
[7] C. Sun, J. Deng, S. M. Rafi-Ul-Islam, G. Liang, H. Yang, and M. B. A. Jalil, Phys. Rev. Appl. **12**, 034022 (2019).
[8] S. Meyer, Y.-T. Chen, S. Wimmer, M. Althammer, T. Wimmer, R. Schlitz, S. Geprägs, H. Huebl, D. Ködderitzsch, H. Ebert, G. E. W. Bauer, R. Gross, and S. T. B. Goennenwein, Nat. Mater. **16**, 977 (2017).
[9] S. Wimmer, D. Ködderitzsch, K. Chadova, and H. Ebert, Phys. Rev. B **88**, 201108(R) (2013).
[10] P. Sheng, Y. Sakuraba, Y.-C. Lau, S. Takahashi, S. Mitani, and M. Hayashi, Sci. Adv. **3**, e1701503 (2017).
[11] A. Bose, S. Bhuktare, H. Singh, S. Dutta, V. Achanta, and A. Tulapurkar, Appl. Phys. Lett. **112**, 162401 (2018).
[12] T. Miyasato, N. Abe, T. Fujii, A. Asamitsu, S. Onoda, Y. Onose, N. Nagaosa, and Y. Tokura, Phys. Rev. Lett. **99**, 086602 (2007).
[13] S. Y. Huang, W. G. Wang, S. F. Lee, J. Kwo, and C. L. Chien, Phys. Rev. Lett. **107**, 216604 (2011).
[14] S. N. Guin, K. Manna, J. Noky, S. J. Watzman, C. Fu, N. Kumar, W. Schnelle, C. Shekhar, Y. Sun, J. Gooth, and C. Felser, NPG Asia Mater. **11**, 16 (2019).
[15] K.-I. Uchida, T. Kikkawa, T. Seki, T. Oyake, J. Shiomi, Z. Qiu, K. Takanashi, and E. Saitoh, Phys. Rev. B **92**, 094414 (2015).
[16] Y.-T. Chen, S. Takahashi, H. Nakayama, M. Althammer, S. T. B. Goennenwein, E. Saitoh, and G. E. W. Bauer, Phys. Rev. B **87**, 144411 (2013).
[17] T. Valet and A. Fert, Phys. Rev. B **48**, 7099 (1993).
[18] T. Taniguchi, J. Phys. Soc. Jpn. **85**, 074705 (2016).
[19] J. Barnaś, A. Fert, M. Gmitra, I. Weymann, and V. K. Dugaev, Phys. Rev. B **72**, 024426 (2005).
[20] M. Althammer, S. Meyer, H. Nakayama, M. Schreier, S. Altmannshofer, M. Weiler, H. Huebl, S. Geprägs, M. Opel, R. Gross, D. Meier, C. Klewe, T. Kuschel, J. M. Schmalhorst, G. Reiss, L. Shen, A. Gupta, Y.-T. Chen, G. E. W. Bauer, E. Saitoh, and S. T. B. Goennenwein, Phys. Rev. B **87**, 224401 (2013).
[21] A. Brataas, Y. V. Nazarov, and G. E. Bauer, Eur. Phys. J. B **22**, 99 (2001).
[22] A. Brataas, G. E. Bauer, and P. J. Kelly, Phys. Rep. **427**, 157 (2006).
[23] N. Chung, M. Jalil, and S. Tan, J. Phys. D: Appl. Phys. **42**, 195502 (2009).
[24] C. Sun, Z. B. Siu, S. G. Tan, H. Yang, and M. B. Jalil, J. Appl. Phys. **123**, 153901 (2018).
[25] K. Xia, P. J. Kelly, G. E. W. Bauer, A. Brataas, and I. Turek, Phys. Rev. B **65**, 220401(R) (2002).
[26] Y. Sakuraba, Scr. Mater. **111**, 29 (2016).
[27] J. Bass and W. P. Pratt, Jr., J. Phys.: Condens. Matter **19**, 183201 (2007).
[28] K. Uchida, S. Takahashi, J. Ieda, K. Harii, K. Ikeda, W. Koshibae, S. Maekawa, and E. Saitoh, J. Appl. Phys. **105**, 07C908 (2009).
[29] M. Isasa, E. Villamor, L. E. Hueso, M. Gradhand, and F. Casanova, Phys. Rev. B **91**, 024402 (2015).
[30] T. Yoshino, K. Ando, K. Harii, H. Nakayama, Y. Kajiwara, and E. Saitoh, J. Phys.: Conf. Ser. **266**, 012115 (2011).
[31] C. Swindells, A. T. Hindmarch, A. J. Gallant, and D. Atkinson, Phys. Rev. B **99**, 064406 (2019).
[32] H. Nakayama, M. Althammer, Y.-T. Chen, K. Uchida, Y. Kajiwara, D. Kikuchi, T. Ohtani, S. Geprägs, M. Opel, S. Takahashi, R. Gross, G. E. W. Bauer, S. T. B. Goennenwein, and E. Saitoh, Phys. Rev. Lett. **110**, 206601 (2013).
[33] S. Cho, S. H. Baek, K. D. Lee, Y. Jo, and B. G. Park, Sci. Rep. **5**, 14668 (2015).
[34] J. Kim, J. Sinha, M. Hayashi, M. Yamanouchi, S. Fukami, T. Suzuki, S. Mitani, and H. Ohno, Nat. Mater. **12**, 240 (2013).
[35] P. He, X. Qiu, V. L. Zhang, Y. Wu, M. H. Kuok, and H. Yang, Adv. Electron. Mater. **2**, 1600210 (2016).
[36] Y. Cheng, K. Chen, and S. Zhang, Appl. Phys. Lett. **112**, 052405 (2018).
[37] P. M. Haney, H.-W. Lee, K.-J. Lee, A. Manchon, and M. D. Stiles, Phys. Rev. B **87**, 174411 (2013).
[38] V. P. Amin and M. D. Stiles, Phys. Rev. B **94**, 104420 (2016).
[39] C. Bilzer, Ph.D. dissertation, Université Paris-Sud, 2007.
[40] H. Xi, Y. Shi, and K.-Z. Gao, J. Appl. Phys. **97**, 033904 (2005).
[41] A. J. Schellekens, K. C. Kuiper, R. R. J. C. de Wit, and B. Koopmans, Nat. Commun. **5**, 4333 (2014).
[42] T. Chiba, G. E. W. Bauer, and S. Takahashi, Phys. Rev. Appl. **2**, 034003 (2014).
[43] D. Fang, H. Kurebayashi, J. Wunderlich, K. Výborný, L. P. Zârbo, R. P. Campion, A. Casiraghi, B. L. Gallagher, T. Jungwirth, and A. J. Ferguson, Nat. Nanotechnol. **6**, 413 (2011).
[44] H. Kubota, A. Fukushima, K. Yakushiji, T. Nagahama, S. Yuasa, K. Ando, H. Maehara, Y. Nagamine, K. Tsunekawa, D. D. Djayaprawira, N. Watanabe, and Y. Suzuki, Nat. Phys. **4**, 37 (2008).
[45] S. Iihama, T. Taniguchi, K. Yakushiji, A. Fukushima, Y. Shiota, S. Tsunegi, R. Hiramatsu, S. Yuasa, Y. Suzuki, and H. Kubota, Nat. Electron. **1**, 120 (2018).